CRYSTAL GROWTH & DESIGN

pubs.acs.org/crystal Article

Epitaxial Synthesis of a Vertically Aligned Two-Dimensional van der Waals Crystal: (110)-Oriented SnO

Matthew Barone,* Chaojie Du, Luka Radosavljevic, Don Werder, Xiaoqing Pan, and Darrell G. Schlom*

Cite This: https://doi.org/10.1021/acs.cgd.2c00905

Read Online

ACCESS | Metrics & More | Article Recommendations | Supporting Information

ABSTRACT: During the explosion of research on two-dimensional (2D) van der Waals crystals over the past couple decades, synthesis has steadily advanced to include epitaxial films but always with the low-energy plane of the 2D material parallel to the surface of the substrate. Here, we report epitaxial synthesis of a 2D van der Waals crystal, SnO, in which the layers are aligned perpendicular to the surface. This accomplishment is particularly important for SnO, a top candidate *p*-type transparent conducting oxide, because the crystallographic direction with the highest hole mobility lies in the plane of the film where it could be utilized in a transistor. We find that the discontinuous nanowire morphology of the films prevents fabrication of useful devices, but nonetheless, this discovery represents a milestone in the fields of 2D materials synthesis and *p*-type oxides.

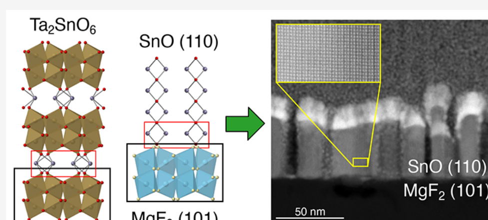

■ INTRODUCTION

In the field of oxide electronics, few discoveries would be more disruptive than the demonstration of a scalable, high-mobility *p*-type oxide for thin-film transistors.[1−5] While there are demonstrations of *n*-channel oxide devices with high mobility using numerous materials,[6−10] the complementary *p*-channel oxide devices lag behind due to various challenges. Most notably, *p*-type oxides with high hole mobility are rare because the top of the valence band is often dominated by oxygen 2p orbitals in metal oxides. These orbitals are relatively localized compared to the metal orbitals that make up the bottom of the conduction band, meaning that the effective mass of holes at the valence band edge tends to be much higher than those of electrons at the conduction band edge.[11] Metal suboxides (e.g., Cu_2O,[12−16] SnO,[17−24] and NiO[25−27]) represent many of the most promising *p*-type oxides because they have filled metal orbitals with relatively high energy that can hybridize with oxygen 2p orbitals to increase the dispersion of the valence band, reducing the hole effective mass. Furthermore, these phases can often accommodate an excess of oxygen enabling *p*-type conductivity without extrinsic dopants.[13] Nevertheless, suboxides have a relatively small range of oxygen chemical potentials for which they are thermodynamically stable. For example, when trying to synthesize Cu_2O, if the oxygen chemical potential is too low, Cu metal will form, and if the oxygen chemical potential is too high, Cu will be over oxidized to CuO. This challenge contrasts with prominent *n*-type oxides, such as In_2O_3, for which highly oxidizing conditions can be employed without fear of over-oxidation, simplifying the synthesis.

Even within the relatively narrow range of oxygen chemical potentials for which *p*-type suboxides are stable, spontaneous formation of compensating defects can prevent the formation of mobile holes. For example, oxygen vacancies are often low-energy defects that can trap would-be holes preventing *p*-type conduction, and such compensating defects become increasingly favorable as more holes are introduced, which can result in their spontaneous formation at useful carrier concentrations.[1,13,28−31] Another major challenge is interfacial traps that pin the Fermi energy. These can cause films with promising hole mobilities by Hall measurements to become useless for electric devices.[12] These challenges, and others, have stymied the discovery of useful *p*-type oxides, hampering the development of transparent electronics[2−4] and a low-power analogue of complementary metal oxide semiconductor technology at back-end-of-the-line temperatures for transistors.[32]

One of the most promising *p*-type oxides is SnO. In this material, filled Sn 5s orbitals hybridize with O 2p orbitals to form the top of the valence band, resulting in much more dispersion, meaning a lower effective mass and a higher mobility. Furthermore, unlike many candidate *p*-type oxides for which appreciable hole doping has proven difficult or impossible due to spontaneous formation of compensating defects[1,13,28−31] or interfacial traps,[12] holes with mobility >5 $cm^2/(V{\cdot}s)$ have been demonstrated in SnO using an electric field effect, intrinsic, and extrinsic dopants.[17−24] Using field effect, hole mobilities as high as 10.8 $cm^2/(V{\cdot}s)$ have been

Received: August 9, 2022
Revised: November 3, 2022

Downloaded via CORNELL UNIV on November 30, 2022 at 20:22:15 (UTC).
See https://pubs.acs.org/sharingguidelines for options on how to legitimately share published articles.

measured in nanocrystalline SnO with processing temperatures <200 °C.[20] Hall effect measurements have revealed room-temperature hole mobilities as high as 30 $cm^2/(V·s)$ in bulk, polycrystalline SnO[23] and as high as 21 $cm^2/(V·s)$ in epitaxial SnO.[24] One possible explanation for the superior hole mobility in polycrystalline SnO is that all demonstrated epitaxial SnO films are (001)-oriented.[17,21,24,33] Hu et al. calculate the hole mobility tensor, μ_{ij}, of SnO at room temperature to be $\mu_{ij} = \begin{pmatrix} 7.4 & 0 & 0 \\ 0 & 7.4 & 0 \\ 0 & 0 & 60.0 \end{pmatrix} \frac{\text{cm}^2}{\text{V s}}$,[22] meaning that the theoretical room-temperature in-plane hole mobility of (001)-oriented SnO films (7.4 $cm^2/(V·s)$) is drastically lower than that along the *c* axis (60 $cm^2/(V·s)$) at room temperature.[22] Minohara et al.[34] report that this theoretical calculation underestimates the room-temperature hole mobility that is experimentally observed in (001)-oriented films.The measurements of Monohara et al.[3434] reveal by angle-resolved photoemission spectroscopy (ARPES) that the valence band is more dispersive than that calculated in ref 22, resulting in underestimation of the hole mobility by theory. Nevertheless, these ARPES measurements confirm that the hole effective mass along the *c* axis is markedly lower than that in the (001) plane,[34] suggesting that the hole mobility is maximized along the *c* axis in qualitative agreement with theoretical predictions.[22] In a polycrystalline sample, some of the grains are aligned with the high-mobility *c* axis parallel to the current, but all demonstrated epitaxial samples are (001)-oriented,[17,21,24,33] the worst orientation imaginable.

Of course, to maximize in-plane mobility, SnO should be grown epitaxially with the high-mobility *c* axis in the plane of the film, but no such synthesis has been reported despite widespread interest in *p*-type SnO. In practice, a film with the high-mobility *c* axis lying in the plane is difficult to realize because the litharge structure of SnO has weak van der Waals bonding between layers in the (001) plane, meaning that a (001)-oriented film has by far the lowest surface energy.[35] While vertically aligned transition metal dichalcogenides with random in-plane texturing have been demonstrated,[36] an epitaxial film of a van der Waals material with the layers aligned perpendicular to the surface in a fixed orientation is completely unprecedented. If possible, not only would such a film enable measurement and utilization of previously inaccessible material properties (e.g., SnO mobility along the *c* axis), but a vertically aligned 2D material would be a fascinating platform for intercalation experiments.[37]

In this work, we demonstrate synthesis of epitaxial (110)-oriented SnO by utilizing (101)-oriented rutile MgF_2 substrates. Through epitaxial synthesis of this vertically aligned van der Waals material, we successfully place the high-mobility *c* axis in the plane of the film. While this orientation of SnO is far more attractive in theory, the films are fairly insulating because they self-assemble into a forest of epitaxial nanowires. While we were unable to make use of (110)-oriented SnO to fabricate high-mobility transistors, we hope that our work will motivate further research to improve the morphology, study intercalation,[37] or use the nanowires to make epitaxial composite films[38−40] to expose new properties.

■ METHODS

Thin films of SnO were synthesized by molecular-beam epitaxy (MBE) in a Veeco GEN10. SnO was supplied from an effusion cell containing SnO_2 powder, from which SnO is the most volatile species.[37] The SnO_2 source was operated at a temperature of 965 °C, which produced a molecular flux of approximately 3.5×10^{13} molecules/(cm^2•s) at an angle of approximately 40° from the surface normal. Growth was performed at a background chamber pressure of 1×10^{-6} Torr O_2 and using substrate temperatures ranging from 310 to 400 °C as measured by a thermocouple near but not in contact with the substrate. X-ray diffraction (XRD) spectra were collected with a Panalytical Empyrean diffractometer using Cu-$K_{\alpha1}$ radiation, and atomic force microscopy (AFM) was performed using an Asylum Cipher ES Environmental AFM.

■ RESULTS

As for many candidate *p*-type oxides, one challenge of synthesizing SnO is isolating the intermediate oxidation state, which has a limited range of stability (i.e., suppressing reduction to β-Sn or oxidation to SnO_2).[41,42] This problem has previously been overcome by using the SnO molecular beam generated by an SnO_2 source.[21,31,43,44] From thermodynamic calculations,[43] the molecular beam produced by heating SnO_2 (or a two-phase mixture of SnO_2 (s) + Sn (l)) should be 99.9% SnO (g) molecules, and this has been observed experimentally using mass spectrometry.[44] By starting with an SnO molecular beam, the phase has been kinetically stabilized to grow (001)-oriented SnO films by MBE,[21] and we employ the same strategy here to grow (110)-oriented SnO films.

To stabilize the (110) orientation of SnO, substrate selection is essential. (001)-Oriented SnO will always have lower surface energy than (110)-oriented SnO, so a substrate that has exceptionally low interfacial energy with (110)-oriented SnO is required. We draw inspiration from the Ta_2SnO_6 thoreaulite crystal structure comprised of alternating Ta_2O_5 and SnO layers (Figure 1a). As first noted by Katayama

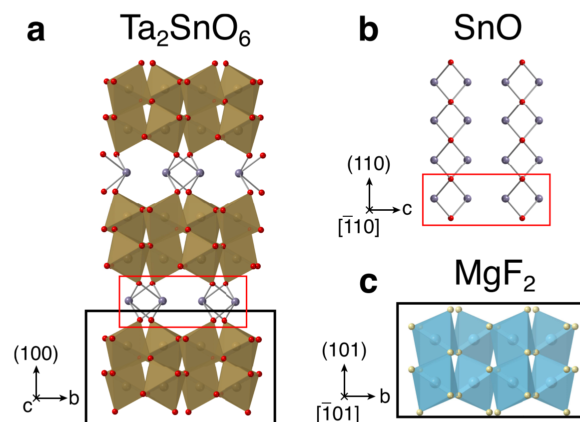

Figure 1. Crystal structure schematics of (a) Ta_2SnO_6, (b) SnO, and (c) MgF_2. Sn^{2+}, O^{2-}, and F^- ions are depicted by purple, red, and beige spheres, respectively. TaO_6 and MgF_6 octahedra are colored brown and blue, respectively. The normal to the plane of the film and the in-plane directions are specified for each material.

et al.,[29] we see in Figure 1 that the SnO surface that bonds to the Ta_2O_5 layers in Ta_2SnO_6 is similar to the (110) surface of pure SnO as indicated by the red boxes in Figure 1, and the Ta_2O_5 layers are structurally similar to (101)-oriented rutile as indicated by the black boxes in Figure 1. Combined, these crystallographic observations of the Ta_2SnO_6 phase suggest that there is an unusually low interfacial energy between the (101) rutile surface and (110) SnO surface. In fact, the lattice mismatch between (110)-oriented SnO and (101)-oriented

https://doi.org/10.1021/acs.cgd.2c00905
Cryst. Growth Des. XXXX, XXX, XXX−XXX

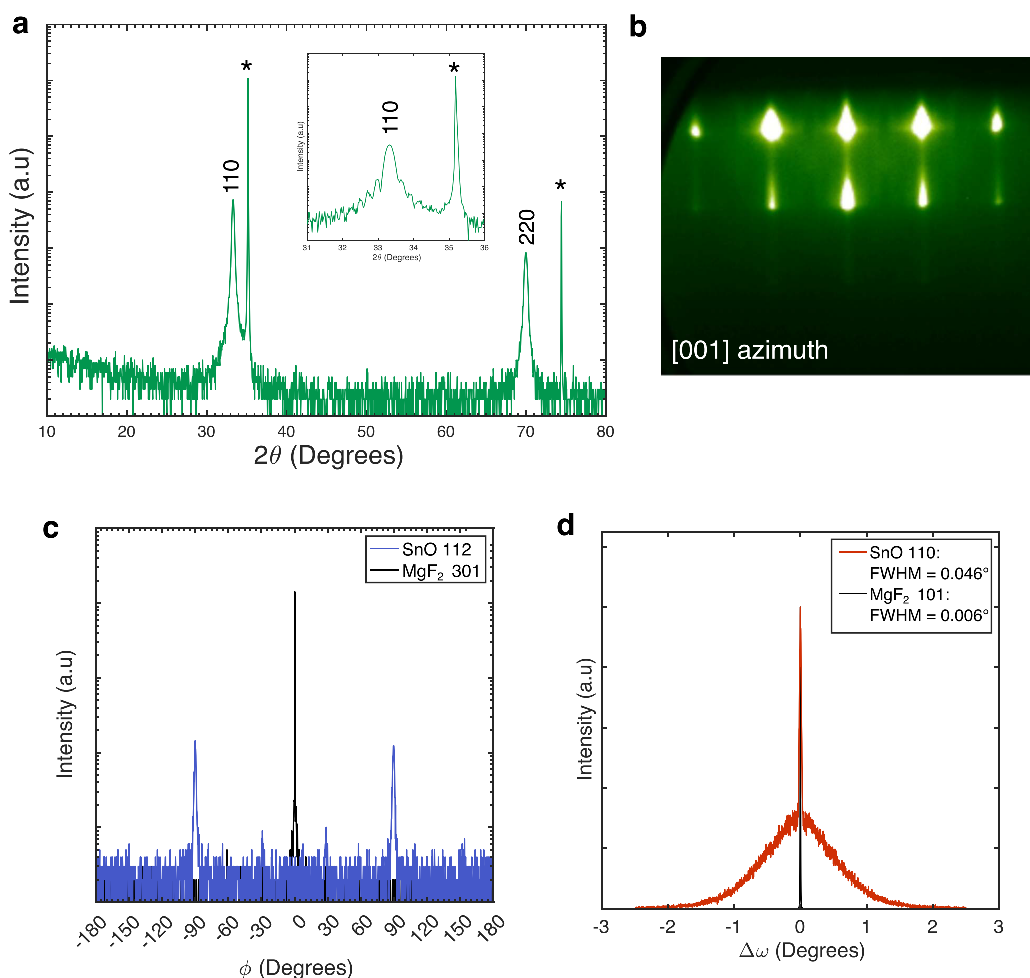

Figure 2. (a) XRD θ−2θ scan of a SnO film grown at a substrate temperature of 330 °C with the inset of a higher resolution scan near the SnO 110 peak. (b) RHEED image collected along the [001] azimuth of SnO after growth of the same film. (c) ϕ scans of the MgF_2 301 peak and the SnO 112 peak. (d) Normalized rocking curves (ω scans) of the MgF_2 101 peak and the SnO 110 peak.

MgF_2 is reasonably low: 4.7% along the [001] direction of SnO and −3.0% along the $[\bar{1}10]$ direction of SnO. Thus, (101)-oriented MgF_2 may be a viable substrate to seed growth of (110)-oriented SnO, and in this orientation, the high-mobility *c* axis of SnO lies in the plane of the film where it could potentially be utilized for a high-mobility transistor.

In Figure 2, we show that synthesis of epitaxial (110)-oriented SnO is possible on a (101)-oriented MgF_2 substrate. The θ−2θ scan in Figure 2a shows no other phases nor orientations, and the high-resolution θ−2θ scan in the inset of Figure 2a reveals Laue oscillations indicating high crystalline quality and a film thickness of 39 nm. The reflection high-energy electron diffraction (RHEED) image (Figure 2b) confirms that the film is epitaxial, albeit quite rough as evidenced by the pattern which more closely resembles transmission electron diffraction than reflection electron diffraction. Based on the θ−2θ scan in Figure 2a and the ϕ scan in Figure 2c, we see that the epitaxial relationship is as expected based on the thoreaulite crystal structure: SnO (110) ∥ MgF_2 (101) and SnO [001] ∥ MgF_2 [010]. Interestingly, the rocking curve in Figure 2d suggests that part of the film has high structural quality resulting in a rocking curve full width at half maximum of 0.046° for the SnO 110 peak. Nonetheless, the rocking curve also shows a broad background signal that has a rocking curve full width at half maximum of ∼1.2° (i.e., if the sharp central peak is ignored). A reciprocal space map (RSM) corroborates the coexistence of broad and sharp diffraction features (Figure 4a). We also find that these (110)-oriented SnO films are quite insulating, with a 2-point resistance of ∼2 MΩ.

To get more insight into these observations, we investigate the morphology of these (110)-oriented SnO films. Annular dark-field scanning transmission electron microscopy (ADF-STEM) and AFM (Figure 3a,c,d, respectively) reveal that SnO self-assembles into a forest of low-symmetry nanowires rather than a continuous film, explaining why the RHEED pattern exhibits features of transmission electron diffraction rather than reflective electron diffraction. The discontinuous morphology also explains why the electrical resistance is so much higher than those of previous reports of unintentionally doped SnO grown by MBE.[21] While the high resistance coupled with the anisotropy of the films makes meaningful electrical characterization challenging, we do consistently observe higher resistance along the *c* axis of SnO than along the $[\bar{1}10]$ direction, which appears to contradict theoretical predictions of the highest mobility being along the *c* axis.[22] Considering the film nanostructure, however, leads us to interpret that the low energy of the SnO (001) surface results in a higher density of voids between SnO crystallites along this direction, which is consistent with AFM (Figure 3c,d), and explains the higher

https://doi.org/10.1021/acs.cgd.2c00905
Cryst. Growth Des. XXXX, XXX, XXX−XXX

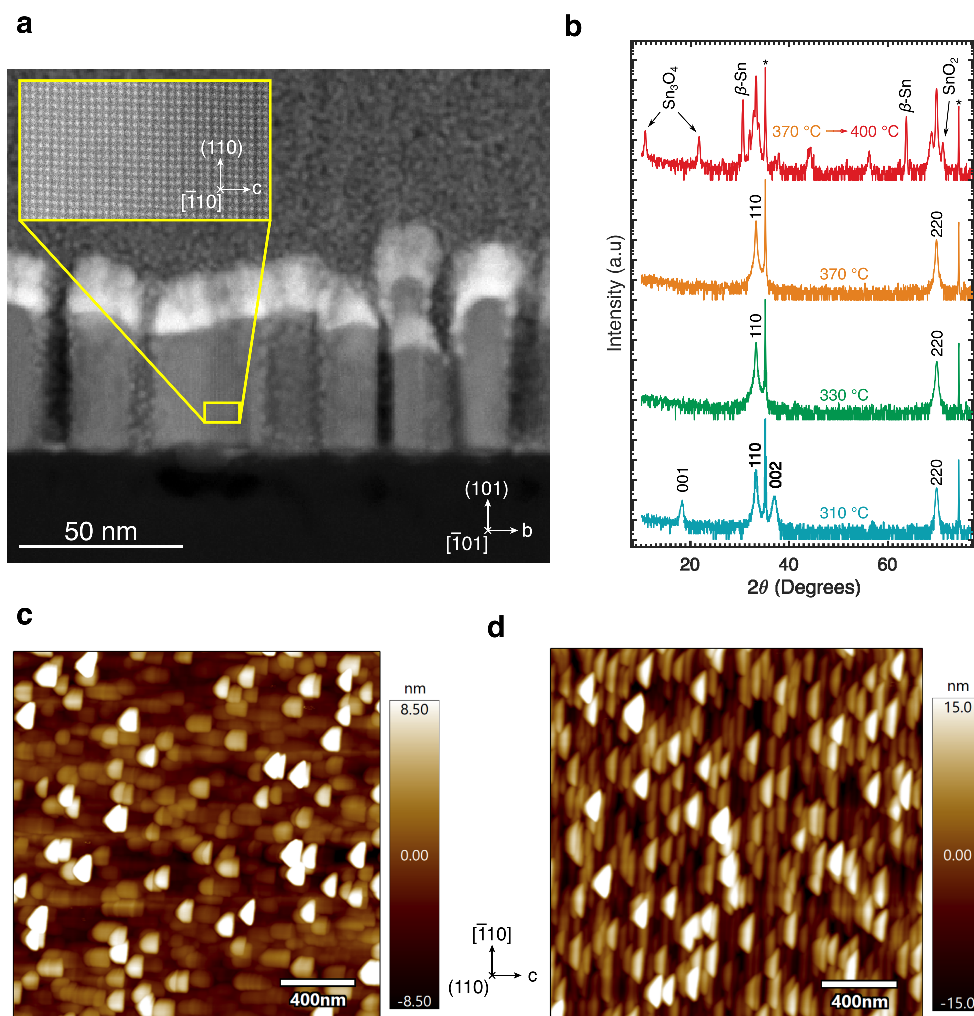

Figure 3. (a) ADF-STEM image of the (110)-oriented SnO film grown at 370 °C. The MgF_2 substrate is at the bottom of the image. The inset shows an atomic-resolution close-up of the SnO film. (b) XRD θ−2θ scans of SnO films grown at substrate temperatures of 310, 330, and 370 °C as well as one that was grown at a substrate temperature of 370 °C and then subsequently annealed in situ at a substrate temperature of 400 °C. (c,d) AFM images of the (110)-oriented SnO films grown at (c) 330 °C and (d) 370 °C with the axes between the images indicating the crystallographic axes of the epitaxial SnO film.

resistance along the [001] direction of SnO. Further STEM imaging revealing a ~5 nm amorphous layer at the interface between SnO and MgF_2 is provided in the Supplemental Information (Figure S1).

One can imagine several strategies to improve the morphology of (110)-oriented SnO films to utilize the high-mobility *c* axis. A potential solution is to use a colder substrate temperature to slow down surface diffusion and kinetically prevent SnO from forming the islands that ultimately seed nanowire growth. We find, however, that lowering the substrate temperature to 310 °C (Figure 3b) results in a mixture of (001)-oriented and (110)-oriented SnO, revealing that if a discontinuous film is kinetically prevented, the system responds by nucleating (001)-oriented SnO rather than forming a continuous film of (110)-oriented SnO. While virtually all incident SnO is desorbed above 400 °C, one could imagine that in situ annealing of nanowires that are nucleated at a substrate temperature of 370 °C may enable coarsening of the SnO (110) nuclei into a continuous film. Unfortunately, when such a film is annealed at 400 °C (Figure 3b), we observe decomposition of the SnO film into a mixture of β-Sn, Sn_3O_4, SnO, and SnO_2, consistent with previous data on the stability of SnO at elevated temperatures.[41] Finally, one could hope that islands would coalesce if the film is grown thick enough, but we have not found this to be the case for film thicknesses as high as 400 nm (see Figure S2).

The morphology observed throughout the (110)-oriented SnO growth window is surprising because the exposed surface area is significantly higher than that of a dense film. Because (110)-oriented SnO nanowires can expose the low-energy (001) surface of SnO, the excess surface energy of the nanowire morphology is abnormally low for (110)-oriented SnO compared to other material systems with more three-dimensional bonding but still ought to be greater than that of a fully dense film. Thus, surface energy arguments are insufficient to fully explain the self-assembly of nanowires on purely thermodynamic grounds. While it is reasonable to expect that the out-of-plane growth rate, i.e., along the [110] direction, is greater than the in-plane growth rate along the *c* axis of SnO due to the higher surface energy of the (110) plane, it remains difficult for us to account for the observation that in-plane growth of SnO nuclei appears to stop completely shortly after the growth begins. Despite careful consideration,

https://doi.org/10.1021/acs.cgd.2c00905
Cryst. Growth Des. XXXX, XXX, XXX−XXX

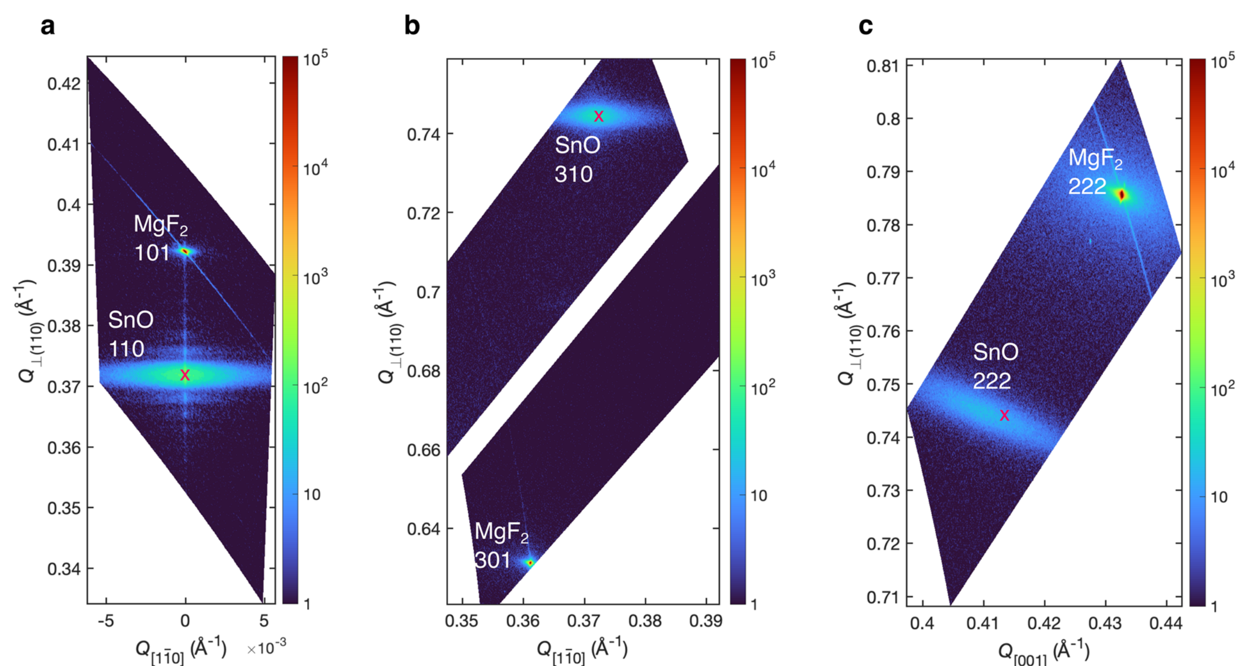

Figure 4. Reciprocal space maps collected near (a) specular MgF_2 101 peak and the SnO 110 peak, (b) MgF_2 301 peak and the SnO 310 peak, and (c) MgF_2 222 peak and the SnO 222 peak. The Miller indices in the axes labels correspond to the SnO lattice (not the MgF_2 lattice), and the expected peak positions for bulk (unstrained) SnO are indicated by red *x*'s.

our explanations remain speculative. We discuss some of these speculative explanations below.

We consider that the nanowires may form to avoid the energetic cost of misfit dislocations, but asymmetric RSMs (Figure 4b,c) reveal that the film is not strained by the substrate. We also consider that translationally offset SnO nuclei may resist coalescence, but 5−10 nm gaps are commonly observed between SnO nanowires in the STEM image in Figure 3a and the AFM images in Figure 3c,d. This distance would appear too large for the neighbor's influence to be felt, but such a mechanism cannot be ruled out. Finally, we note that the SnO molecular beam is incident at 40° from the surface normal of the rotating substrate, which we believe is an important factor. As the SnO nuclei grow upward, they increasingly shadow the exposed MgF_2 from the SnO molecular beam, which further favors perpendicular growth over lateral growth of the SnO nuclei. If the morphology does, in fact, arise from the angle of incidence of the SnO beam, one could attempt to supply an SnO molecular beam perpendicular to the substrate, but this is difficult to accomplish in our system.

CONCLUSIONS

Our report of epitaxial (110)-oriented SnO is relevant to the *p*-type oxide community as well as the field of 2D materials synthesis. Even though SnO is considered among the most promising *p*-type oxides, the authors are unaware of any previous attempts to experimentally confirm predictions that the *c* axis has the highest mobility. While we were ultimately unable to measure the mobility along the *c* axis due to the discontinuous morphology of our films, we hope that our progress will motivate further research to improve the morphology or use the nanowires as the backbone for a composite film. Furthermore, our demonstration of an epitaxial, vertically aligned 2D van der Waals crystal is potentially generalizable to other 2D materials with the litharge structure such as PbO or FeSe. In the case of vertically aligned SnO, we aimed to study the electronic properties perpendicular to the layers, but the orientation and nanostructure of the observed films could also serve as a platform for intercalation experiments or nanowire self-assembly.

ASSOCIATED CONTENT

Supporting Information

The Supporting Information is available free of charge at https://pubs.acs.org/doi/10.1021/acs.cgd.2c00905.

High-magnification STEM image of the film interface and a cross-sectional scanning-electron microscopy (SEM) image of a cleaved 400 nm thick, (110)-oriented SnO film grown on MgF_2 (101) with further speculation on the origin of the nanowire morphology (PDF)

AUTHOR INFORMATION

Corresponding Authors

Matthew Barone − *Department of Materials Science and Engineering, Cornell University, Ithaca, New York 14853, United States;* orcid.org/0000-0003-1221-181X; Email: mrb297@cornell.edu

Darrell G. Schlom − *Department of Materials Science and Engineering, Cornell University, Ithaca, New York 14853, United States; Kavli Institute at Cornell for Nanoscale Science, Ithaca, New York 14853, United States; Leibniz-Institut für Kristallzüchtung, 12489 Berlin, Germany;* orcid.org/0000-0003-2493-6113; Email: schlom@cornell.edu

Authors

Chaojie Du − *Department of Materials Science and Engineering, University of California, Irvine, California 92697, United States*

https://doi.org/10.1021/acs.cgd.2c00905
Cryst. Growth Des. XXXX, XXX, XXX−XXX

Luka Radosavljevic − *Department of Materials Science and Engineering, Cornell University, Ithaca, New York 14853, United States*

Don Werder − *Platform for the Accelerated Realization, Analysis, and Discovery of Interface Materials (PARADIM), Ithaca, New York 14853, United States*

Xiaoqing Pan − *Department of Materials Science and Engineering, University of California, Irvine, California 92697, United States; Irvine Materials Research Institute, University of California, Irvine, California 92697, United States*

Complete contact information is available at:
https://pubs.acs.org/10.1021/acs.cgd.2c00905

Notes

The authors declare no competing financial interest.
The data supporting the findings of this study, as well as additional data related to the growth and structural data, are available within the paper. Any additional data connected to the study are available from the corresponding author upon reasonable request.

■ ACKNOWLEDGMENTS

This work was primarily supported by ASCENT, one of six centers in JUMP, a Semiconductor Research Corporation (SRC) program sponsored by DARPA. Materials synthesis was performed partly in a facility supported by the National Science Foundation [Platform for the Accelerated Realization, Analysis, and Discovery of Interface Materials (PARADIM)] under Cooperative Agreement No. DMR-2039380. This work made use of a Helios FIB supported by NSF (DMR-1539918) and the Cornell Center for Materials Research Shared Facilities which are supported through the NSF MRSEC program (DMR-1719875). Substrate preparation was performed in part at the Cornell NanoScale Facility, a member of the National Nanotechnology Coordinated Infrastructure (NNCI), which is supported by the NSF (Grant No. NNCI-2025233). The authors thank Sean Christopher Palmer for his assistance with substrate preparation. Some images were generated using CrystalMaker: CrystalMaker Software Ltd. (www.crystalmaker.com).

■ REFERENCES

(1) Hautier, G.; Miglio, A.; Ceder, G.; Rignanese, G.-M.; Gonze, X. Identification and Design Principles of Low Hole Effective Mass P-Type Transparent Conducting Oxides. *Nat. Commun.* **2013**, *4*, 2292.
(2) Zhang, K. H. L.; Xi, K.; Blamire, M. G.; Egdell, R. G. P-Type Transparent Conducting Oxides. *J. Phys. Condens. Matter* **2016**, *28*, No. 383002.
(3) Yu, X.; Marks, T. J.; Facchetti, A. Metal Oxides for Optoelectronic Applications. *Nat. Mater.* **2016**, *15*, 383−396.
(4) Petti, L.; Münzenrieder, N.; Vogt, C.; Faber, H.; Büthe, L.; Cantarella, G.; Bottacchi, F.; Anthopoulos, T. D.; Tröster, G. Metal Oxide Semiconductor Thin-Film Transistors for Flexible Electronics. *Appl. Phys. Rev.* **2016**, *3*, No. 021303.
(5) Zhang, Z.; Guo, Y.; Robertson, J. P-Type Semiconduction in Oxides with Cation Lone Pairs. *Chem. Mater.* **2022**, *34*, 643.
(6) Nomura, K.; Ohta, H.; Ueda, K.; Kamiya, T.; Hirano, M.; Hosono, H. Thin-Film Transistor Fabricated in Single-Crystalline Transparent Oxide Semiconductor. *Science* **2003**, *300*, 1269.
(7) Bayraktaroglu, B.; Leedy, K.; Neidhard, R. High-Frequency ZnO Thin-Film Transistors on Si Substrates. *IEEE Electron Device Lett.* **2009**, *30*, 946−948.
(8) Zhou, H.; Maize, K.; Qiu, G.; Shakouri, A.; Ye, P. D. β-Ga_2O_3 on Insulator Field-Effect Transistors with Drain Currents Exceeding 1.5 A/mm and Their Self-Heating Effect. *Appl. Phys. Lett.* **2017**, *111*, No. 092102.
(9) Li, S.; Tian, M.; Gao, Q.; Wang, M.; Li, T.; Hu, Q.; Li, X.; Wu, Y. Nanometre-Thin Indium Tin Oxide for Advanced High-Performance Electronics. *Nat. Mater.* **2019**, *18*, 1091−1097.
(10) Park, J.; Paik, H.; Nomoto, K.; Lee, K.; Park, B. E.; Grisafe, B.; Wang, L. C.; Salahuddin, S.; Datta, S.; Kim, Y.; Jena, D.; Xing, H. G.; Schlom, D. G. Fully Transparent Field-Effect Transistor with High Drain Current and on-off Ratio. *APL Mater.* **2020**, *8*, No. 011110.
(11) Kawazoe, H.; Yasukawa, M.; Hyodo, H.; Kurita, M.; Yanagi, H.; Hosono, H. P-Type Electrical Conduction in Transparent Thin Films of $CuAlO_2$. *Nature* **1997**, *389*, 939−942.
(12) Matsuzaki, K.; Nomura, K.; Yanagi, H.; Kamiya, T.; Hirano, M.; Hosono, H. Epitaxial Growth of High Mobility Cu_2O Thin Films and Application to p -Channel Thin Film Transistor. *Appl. Phys. Lett.* **2008**, *93*, 202107.
(13) Raebiger, H.; Lany, S.; Zunger, A. Origins of the P-Type Nature and Cation Deficiency in Cu_2O and Related Materials. *Phys. Rev. B* **2007**, *76*, No. 045209.
(14) Liao, L.; Yan, B.; Hao, Y. F.; Xing, G. Z.; Liu, J. P.; Zhao, B. C.; Shen, Z. X.; Wu, T.; Wang, L.; Thong, J. T. L.; Li, C. M.; Huang, W.; Yu, T. P-Type Electrical, Photoconductive, and Anomalous Ferromagnetic Properties of Cu_2O Nanowires. *Appl. Phys. Lett.* **2009**, *94*, 113106.
(15) Li, B. S.; Akimoto, K.; Shen, A. Growth of Cu_2O Thin Films with High Hole Mobility by Introducing a Low-Temperature Buffer Layer. *J. Cryst. Growth* **2009**, *311*, 1102−1105.
(16) Yao, Z. Q.; Liu, S. L.; Zhang, L.; He, B.; Kumar, A.; Jiang, X.; Zhang, W. J.; Shao, G. Room Temperature Fabrication of P-Channel Cu_2O Thin-Film Transistors on Flexible Polyethylene Terephthalate Substrates. *Appl. Phys. Lett.* **2012**, *101*, No. 042114.
(17) Ogo, Y.; Hiramatsu, H.; Nomura, K.; Yanagi, H.; Kamiya, T.; Hirano, M.; Hosono, H. P-Channel Thin-Film Transistor Using p -Type Oxide Semiconductor SnO. *Appl. Phys. Lett.* **2008**, *93*, No. 032113.
(18) Fortunato, E.; Barros, R.; Barquinha, P.; Figueiredo, V.; Park, S. H. K.; Hwang, C. S.; Martins, R. Transparent P-Type SnO_x Thin Film Transistors Produced by Reactive Rf Magnetron Sputtering Followed by Low Temperature Annealing. *Appl. Phys. Lett.* **2010**, *97*, No. 052105.
(19) Liang, L. Y.; Liu, Z. M.; Cao, H. T.; Yu, Z.; Shi, Y. Y.; Chen, A. H.; Zhang, H. Z.; Fang, Y. Q.; Sun, X. L. Phase and Optical Characterizations of Annealed SnO Thin Films and Their P-Type TFT Application. *J. Electrochem. Soc.* **2010**, *157*, H598.
(20) Caraveo-Frescas, J. A.; Alshareef, H. N. Transparent P-Type SnO Nanowires with Unprecedented Hole Mobility among Oxide Semiconductors. *Appl. Phys. Lett.* **2013**, *103*, 222103.
(21) Mei, A. B.; Miao, L.; Wahila, M. J.; Khalsa, G.; Wang, Z.; Barone, M.; Schreiber, N. J.; Noskin, L. E.; Paik, H.; Tiwald, T. E.; Zheng, Q.; Haasch, R. T.; Sangiovanni, D. G.; Piper, L. F. J.; Schlom, D. G. Adsorption-Controlled Growth and Properties of Epitaxial SnO Films. *Phys. Rev. Mater.* **2019**, *3*, No. 105202.
(22) Hu, Y.; Hwang, J.; Lee, Y.; Conlin, P.; Schlom, D. G.; Datta, S.; Cho, K. First Principles Calculations of Intrinsic Mobilities in Tin-Based Oxide Semiconductors SnO, SnO_2, and Ta_2SnO_6. *J. Appl. Phys.* **2019**, *126*, 185701.
(23) Miller, S. A.; Gorai, P.; Aydemir, U.; Mason, T. O.; Stevanović, V.; Toberer, E. S.; Snyder, G. J. SnO as a Potential Oxide Thermoelectric Candidate. *J. Mater. Chem. C* **2017**, *5*, 8854−8861.
(24) Minohara, M.; Samizo, A.; Kikuchi, N.; Bando, K. K.; Yoshida, Y.; Aiura, Y. Tailoring the Hole Mobility in SnO Films by Modulating the Growth Thermodynamics and Kinetics. *J. Phys. Chem. C* **2020**, *124*, 1755−1760.
(25) Adler, D.; Feinleib, J. Electrical and Optical Properties of Narrow-Band Materials. *Phys. Rev. B* **1970**, *2*, 3112−3134.

https://doi.org/10.1021/acs.cgd.2c00905
Cryst. Growth Des. XXXX, XXX, XXX−XXX

(26) Sato, H.; Minami, T.; Takata, S.; Yamada, T. Transparent Conducting P-Type NiO Thin Films Prepared by Magnetron Sputtering. *Thin Solid Films* **1993**, *236*, 27−31.
(27) He, J.; Lindström, H.; Hagfeldt, A.; Lindquist, S.-E. Dye-Sensitized Nanostructured p-Type Nickel Oxide Film as a Photocathode for a Solar Cell. *J. Phys. Chem. B* **1999**, *103*, 8940−8943.
(28) Robertson, J.; Clark, S. J. Limits to Doping in Oxides. *Phys. Rev. B* **2011**, *83*, 75205.
(29) Katayama, S.; Hayashi, H.; Kumagai, Y.; Oba, F.; Tanaka, I. Electronic Structure and Defect Chemistry of Tin(II) Complex Oxide $SnNb_2O_6$. *J. Phys. Chem. C* **2016**, *120*, 9604−9611.
(30) Dahliah, D.; Rignanese, G.-M.; Hautier, G. Defect Compensation in the P-Type Transparent Oxide Ba_2BiTaO_6. *J. Mater. Chem. C* **2020**, *8*, 9352−9357.
(31) Barone, M.; Foody, M.; Hu, Y.; Sun, J.; Frye, B.; Perera, S. S.; Subedi, B.; Paik, H.; Hollin, J.; Jeong, M.; Lee, K.; Winter, C. H.; Podraza, N. J.; Cho, K.; Hock, A.; Schlom, D. G. Growth of Ta_2SnO_6 Films, a Candidate Wide-Band-Gap p-Type Oxide. *J. Phys. Chem. C* **2022**, *126*, 3764−3775.
(32) Salahuddin, S.; Ni, K.; Datta, S. The Era of Hyper-Scaling in Electronics. *Nat. Electron.* **2018**, *1*, 442−450.
(33) Minohara, M.; Kikuchi, N.; Yoshida, Y.; Kumigashira, H.; Aiura, Y. Improvement of the Hole Mobility of SnO Epitaxial Films Grown by Pulsed Laser Deposition. *J. Mater. Chem. C* **2019**, *7*, 6332−6336.
(34) Minohara, M.; Hase, I.; Aiura, Y. Characteristic Electronic Structure of SnO Film Showing High Hole Mobility. *J. Phys. Chem. Lett.* **2022**, *13*, 1165−1171.
(35) Duan, Y. Electronic Properties and Stabilities of Bulk and Low-Index Surfaces of SnO in Comparison with SnO_2: A First-Principles Density Functional Approach with an Empirical Correction of van Der Waals Interactions. *Phys. Rev. B* **2008**, *77*, No. 045332.
(36) Kong, D.; Wang, H.; Cha, J. J.; Pasta, M.; Koski, K. J.; Yao, J.; Cui, Y. Synthesis of MoS_2 and $MoSe_2$ Films with Vertically Aligned Layers. *Nano Lett.* **2013**, *13*, 1341−1347.
(37) Hu, Y.; Schlom, D.; Datta, S.; Cho, K. Interlayer Engineering of Band Gap and Hole Mobility in P-Type Oxide SnO. *ACS Appl. Mater. Interfaces* **2022**, *14*, 25670−25679.
(38) Zheng, H.; Wang, J.; Mohaddes-Ardabili, L.; Wuttig, M.; Salamanca-Riba, L.; Schlom, D. G.; Ramesh, R. Three-Dimensional Heteroepitaxy in Self-Assembled $BaTiO_3-CoFe_2O_4$ Nanostructures. *Appl. Phys. Lett.* **2004**, *85*, 2035−2037.
(39) MacManus-Driscoll, J. L.; Suwardi, A.; Wang, H. Composite Epitaxial Thin Films: A New Platform for Tuning, Probing, and Exploiting Mesoscale Oxides. *MRS Bull.* **2015**, *40*, 933−942.
(40) Prakash, A.; Wang, T.; Bucsek, A.; Truttmann, T. K.; Fali, A.; Cotrufo, M.; Yun, H.; Kim, J.-W.; Ryan, P. J.; Mkhoyan, K. A.; Alù, A.; Abate, Y.; James, R. D.; Jalan, B. Self-Assembled Periodic Nanostructures Using Martensitic Phase Transformations. *Nano Lett.* **2021**, *21*, 1246−1252.
(41) Cahen, S.; David, N.; Fiorani, J. M.; Maître, A.; Vilasi, M. Thermodynamic Modelling of the O-Sn System. *Thermochim. Acta* **2003**, *403*, 275−285.
(42) Hu, Y.; Yao, X.; Schlom, D. G.; Datta, S.; Cho, K. First Principles Design of High Hole Mobility P-Type Sn-O-X Ternary Oxides: Valence Orbital Engineering of Sn^{2+} in Sn^{2+}-O-X by Selection of Appropriate Elements X. *Chem. Mater.* **2021**, *33*, 212−225.
(43) Adkison, K. M.; Shang, S. L.; Bocklund, B. J.; Klimm, D.; Schlom, D. G.; Liu, Z. K. Suitability of Binary Oxides for Molecular-Beam Epitaxy Source Materials: A Comprehensive Thermodynamic Analysis. *APL Mater.* **2020**, *8*, No. 081110.
(44) Hoffmann, G.; Budde, M.; Mazzolini, P.; Bierwagen, O. Efficient Suboxide Sources in Oxide Molecular Beam Epitaxy Using Mixed Metal + Oxide Charges: The Examples of SnO and Ga_2O. *APL Mater.* **2020**, *8*, No. 031110.

https://doi.org/10.1021/acs.cgd.2c00905
Cryst. Growth Des. XXXX, XXX, XXX−XXX